

UNIVERSITI
TEKNOLOGI
PETRONAS
engineering for all

CFD Modelling of Bubble-Bubble Coalescence

by

Zalinawati binti Zakaria

(8519)

Supervisor: Dr. Nurul Hasan

Dissertation submitted in partial fulfilment of
the requirements for the
Bachelor of Engineering (Hons)
(Chemical Engineering)

JUNE 2010

Universiti Teknologi PETRONAS
Bandar Seri Iskandar
31750 Tronoh
Perak Darul Ridzuan

CERTIFICATION OF APPROVAL

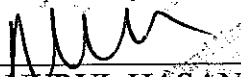
CFD Modelling of Bubble-Bubble Coalescence

by

Zalinawati binti Zakaria
(8519)

A project dissertation submitted to the
Chemical Engineering Programme
Universiti Teknologi PETRONAS
in partial fulfilment of the requirement for the
BACHELOR OF ENGINEERING (Hons)
(CHEMICAL ENGINEERING)

Approved by,


DR. NURUL HASAN

UNIVERSITI TEKNOLOGI PETRONAS

TRONOH, PERAK

June 2010

CERTIFICATION OF ORIGINALITY

This is to certify that I am responsible for the work submitted in this project, that the original work is my own except as specified in the references and acknowledgements, and that the original work contained herein have not been undertaken or done by unspecified sources or persons.

Zalini

ZALINAWATI BINTI ZAKARIA

ACKNOWLEDGEMENT

In the name of Allah, the Most Gracious, the Most Merciful. Praise to Him the Almighty that in his will and given strength, had I managed to complete my Final Year Project within the given period. A lot has transpired during this period of time and I am in debt to so many who had made this to become a successful project.

Hereby, I would like to express my utmost gratitude and appreciation to my FYP Supervisor, Dr. Nurul Hasan for his enlightening supervision and countless hours spent in sharing his insightful understanding, profound knowledge and valuable experiences throughout my project.

Special thanks go to the course coordinator, Dr Khalik bin Mohd Sabil for his guidance and advices. My deepest gratitude also goes to all examiners for their kind evaluation and precious time.

I also like to acknowledge my appreciation to my family for giving a continuous support until the completion of this project. Last but not least, my sincere and heartfelt gratitude is dedicated to all my fellow friends who have directly or indirectly lent a helping hand. Thank you.

ABSTRACT

The content of this report summarizes the outcome of the CFD Modelling of Bubble-bubble Coalescence project. The main project objective is to investigate the dynamics of coalescence process of two co-axial bubbles within liquid phase under laminar flow condition. Computational Fluid Dynamics (CFD) software has been used in this project to simulate the coalescence process which focuses on 3-dimensional simulation. In many engineering process, it is founded that a lack of understanding in bubble coalescence mechanism will complicate the study of dispersion process and mass transfer mechanisms to optimize equipment design. Thus it is important to understand the bubble coalescence behaviours that can lead to the change of bubble size distributions in controlling mass transfer between gas and liquid. This project deals with multiphase flow which is gas-liquid flow. The modelling approach selected is Volume-of-Fluid method (VOF) which commonly used to analyse the dynamic and deformation of the liquid-gas interface. The main tool required in this project is FLUENT which is CFD software and other software have been used are GAMBIT and AutoCAD.. Based on the numerical result, the analysis was done to visualize coalescence mechanism which can be described into three consecutive steps; (1) collision of bubbles, (2) trapping and thinning of a thin liquid film and (3) film rupture. This agrees with the description given by Oolman, T. O. and Blanch, H. W., 1986. Futhermore, the effect of surface tension on the coalescence have been studied as one of the objectives. From the result, a high surface tension is observed to produce a weak liquid jet behind the bubbles and the resultant high surface tension force prohibits the surface stretching. These all cause a late coalescence to occur. In addition, from the result generated by CFD, the bubble trajectories can be plotted accurately and such an information should be helpful in hydrodynamics modelling of bubbly flows. In conclusion, the mechanism of coalescence can be investigated using CFD software and the project objectives are satisfied.

TABLE OF CONTENTS

ABSTRACT		i
CHAPTER 1:	INTRODUCTION	1
	1.1 Background of Study	1
	1.2 Problem Statement	2
	1.3 Objectives	3
	1.4 Scope of Study	4
CHAPTER 2:	LITERATURE REVIEW	5
	2.1 Bubble-Bubble Coalescence	5
	2.2 Bubble Transport	7
	2.3 Available Related Models	9
	2.4 Computational Fluid Dynamics	11
	2.5 Volume-of-Fluid (VOF) Model	13
	2.6 Modelling Case Overview	15
CHAPTER 3:	METHODOLOGY	18
	3.1 Project Flow Chart	18
	3.2 Project Work Execution	19
	3.3 Project Gantt Chart	20
	3.4 Tools and Equipment	21
CHAPTER 4:	RESULT AND DISCUSSION	22
	4.1 The Behavior of Bubble Coalescence	22
	4.2 The Effect of Surface Tension on Bubble Coalescence	28
CHAPTER 5:	CONCLUSION AND RECOMMENDATION	39
	5.1 Conclusion	39
	5.2 Recommendation	40
REFERENCES		41
APPENDICES		44
	Appendix A: Specific Heat Ratio of Air	44

LIST OF FIGURES

Figure 2.1	: Consecutive steps in bubble-bubble coalescence	6
Figure 2.2	: Schematic diagram of co-axial bubbles	7
Figure 2.6.1	: Schematic diagram of apparatus	16
Figure 2.6.2	: Predicted axisymmetric coalescence of two gas bubbles in a viscous liquid	17
Figure 2.6.3	: Experimental observation of the axisymmetric coalescence of two gas bubbles in a glycerin liquid	17
Figure 3.1	: Project flow chart	18
Figure 3.2	: Project work execution	19
Figure 3.3.1	: Gantt chart of FYP 1	20
Figure 3.3.2	: Gantt chart of FYP 2	20
Figure 4.1.1	: Computational domain	24
Figure 4.1.2	: Series of contours of volume fraction	26
Figure 4.1.3	: Position of two bubbles as a function of time	27
Figure 4.2.1	: Computational domain	32
Figure 4.2.2	: Predicted axisymmetric coalescence (Case 1)	33
Figure 4.2.3	: Simulated axisymmetric coalescence (Case 1)	34
Figure 4.2.4	: Predicted axisymmetric coalescence (Case 2)	36
Figure 4.2.5	: Simulated axisymmetric coalescence (Case 2)	36
Figure 4.2.6	: Position of two bubbles as a function of time (Case 1)	37
Figure 4.2.7	: Position of two bubbles as a function of time (Case 2)	37
Figure 4.2.8	: Position of two bubbles as a function of time (Case 3)	38

LIST OF TABLES

Table 2.3.1	: Available literature models for the coalescence time in pure liquids	10
Table 2.3.2	: Influence of liquid properties on the bubble diameter	11
Table 4.1	: Boundary conditions and fluid properties	25
Table 4.2.1	: Real time data	30
Table 4.2.2	: Boundary conditions and fluid properties	31
Table 4.2.3	: Parameters for simulation test cases	33

CHAPTER 1

INTRODUCTION

1.1 Background of Study

In chemical engineering application and industry, many processes involve with multiphase flows. For gas-liquid two phase systems, it incorporates contact of a dispersed gaseous phase and a continuous liquid phase where mass transfer takes place. The specific interfacial area is a very important parameter in determining the mass transfer rate and thus the evolution of the bubble size distribution needs to be concerned about (E. I. V. van de Hengel et al., 2005). Processes such as bubble breakup and coalescence can greatly influence the overall performance by altering the interfacial area available for mass transfer between the phases (Katerina A. Mouza et al., 2004). For instance, in mixing, bubbles or drops can generate large changes in interfacial areas through the action of vorticity via stretching, tearing and folding which facilitates the mixing processes (Li Chen et al., 1998).

The knowledge about bubbly flows is essential in optimizing gas-liquid equipment design such as bubble columns which are widely used in various industry applications. In spite of the widespread application of bubble columns and substantial research efforts devoted to understand their behavior, detailed knowledge on bubbles breakup and coalescence is lacking and is often ignored in hydrodynamic modelling (E. I. V. van de Hengel et al., 2005). Krishna and Van Baten in their research considered a three-phase continuum and assumed that bubbles in the column were either 'small' or 'large', with different velocities, but with no interaction between the bubbles (Katerina A. Mouza et al., 2004). However, considering the higher superficial gas velocities that usually encounter in real industry situation, the interaction factors should be taken into account to gain better insight in the hydrodynamics of bubbly flows.

In addition, the field of microfluidics has experienced a rapid development in the past few years, being reflected in a number of emerging technologies such as micropumps, lab-on-a-chip systems, or chemical microreactors (S. Hardt, 2005). Furthermore, a study in microchannel geometries for two phase flows currently has drew interest and recent experimental results indicates that the droplets can be in close contact without undergoing coalescence (Todd Thorsen et al., 2001). This observation is contradict to a number of existing numerical predictions for microscale free-surface flow and S. Hardt (2005) in his study has developed a formula allowing to take into account the interaction of the fluid interface in computational methods for free surface flow.

1.2 Problem Statement

The dynamics of bubble coalescence plays a significant role in gas-liquid system which contributes to the changes of bubbly flow dynamics. A lack of understanding in bubble coalescence mechanism will complicate the study of dispersion and mass transfer process to optimize equipment design such as bubble column reactors. In order to have a sufficient knowledge, the key is to investigate the factors or parameters which affect the fluid dynamics depending on the nature of the process. For an example, microflows are usually dominated by surface effects such as surface-tension forces or the formation of electric double layers; dissimilar with macroscopic flows (S. Hardt, 2005).

In this Final Year Project, it is not attempted to consider the multiple interactions of bubbles in the large scale geometries. At this level, comprehension on a single interaction of a pair bubbles will be gained for initial understanding. This scope of research corresponds to several established literature that have studied the behaviour of a single and a pair of bubbles with fluid dynamics interactions.

In studying that phenomenon, experiment however cannot serve accurate results for any arbitrary condition due to restrictions to experimental equipment, measurement inaccuracy and measurement system problems. Due to a rapid development in modelling technology nowadays, Computational Fluid Dynamics (CFD) has become as a powerful

tool to simulate the bubble interaction mechanisms because of its predictive capabilities to determine the effect of several bubble properties.

1.3 Objectives

The objectives of the project are stated as following:

- To investigate the dynamics of coalescence process of two co-axial bubbles within liquid phase under laminar flow condition.
- To visualise bubble interaction mechanism and to track the bubble trajectories by using Computational Fluid Dynamics.
- To study the effect of surface tension on bubble coalescence.

The simulation focuses on a case of coalescence process of two bubbles rising co-axially within the liquid phase. From the simulation, the bubble motion will be visualized and be tracked. The problem will be modelled by specifying parameters as further described in Chapter 4 which will help modelling fluid characteristics for this phenomenon.

For this reason, the project works is realised to be feasible within the appropriate time frames. In FYP 1, the works is reserved to perform literature review to study deeply the phenomena of bubble coalescence. A simple two-dimensional simulation of water-air system is performed to gain better insight of the coalescence mechanism and to get familiarize with CFD software. At this level, the subject of interest is to visualize the mechanism steps and to study the fluid behaviour of bubble coalescence process by plotting contours of volume fraction.

For FYP 2, the three-dimensional simulation by using FLUENT is conducted for getting an accurate result to numerically investigate the coalescence process. In this simulation, the trajectory of a pair of bubbles will be tracked and the shape change of coalescence bubble is observed.

1.4 Scope of Study

The project comprises a study of coalescence phenomena in a two phase gas-liquid system. The system under study involves a dynamics of two bubbles contacting each other within the liquid phase in a coalescence cell. In the most existing literature that studied the behaviour of a pair of bubbles, an interaction between the bubbles can be either positioned co-axially or adjacently. Furthermore, the coalescence tank is selected with a simple geometry such as cylinder or rectangular tank to lessen the complexity of the fluid flow analysis.

So far, the gas velocity is not the subject of interest to be incorporated in the modelling as the manipulation parameter. In modelling the framework, several assumptions have been specified to the system as following:

- Laminar and low Reynolds number of flow
- Liquid and gas are isothermal and incompressible
- Two co-axial bubbles with the different radius rising in line
- Bubble is free rising under gravity presence
- Cylindrical tank is used

The project will focus on three-dimensional simulation by using FLUENT software which gives more accurate result of bubbles behaviour. The modelling approach selected in the simulation is Volume-of-Fluid (VOF) method which is a volume-tracking method used to model free surfaces.

CHAPTER 2

LITERATURE REVIEW

2.1 Bubble-Bubble Coalescence

The coalescence is predefined as the process by which two or more bubbles or particles merge during contact to form a single daughter bubble. Collision process between two bubbles may lead either to the coalescence or to bouncing and separation of the bubbles. Looking into the event of coalescence, it can be visualised in several steps. Firstly, the external flow governs whether the bubbles collide, the force of the collision and the contact time (Chesters, A. K., 1991). The consecutive steps in bubble coalescence can be explained within three steps as following (Oolman, T. O. and Blanch, H. W., 1986; Rahman Sudiyo):

a) Collision of bubbles

Two bubbles contact each other within the liquid phase.

b) Trapping and thinning of a thin liquid film

Upon collision impact, there is flattening of the bubbles surfaces in contact, leaving a thin liquid film separating them. This film is typically 10^{-3} and 10^{-4} cm in thickness. Coalescence will take place if the two bubbles stay in contact for longer than is required for the film to thin.

c) Film rupture

Once the film is sufficiently thin, an instability mechanism will result in film rupture and formation of a coalesced bubble. The entire process occurs on a millisecond time scale, the rate determining step being film drainage (Marrucci, G. , 1969).

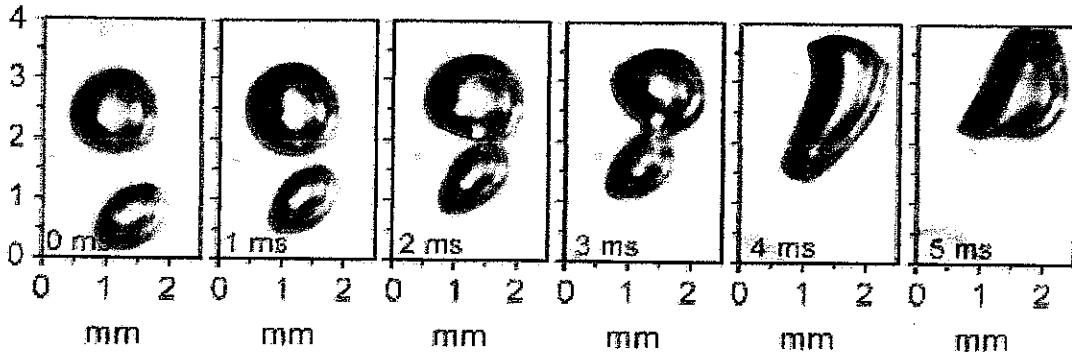


Figure 2.1: Consecutive steps in bubble-bubble coalescence
(Rahman Sudiyo)

Furthermore, whether the coalescence happens or not depends not only on the hydrodynamics and the surface properties but also on the external flow which governs the frequency, force and duration of the collisions (Tse et al., 1998). It is observed based on Figure 2.1 that the time required for two bubbles from the first contact to complete coalescence is about 2ms. The coalescence rate of bubbles is affected by two factors which are the frequency of collision and the probability that bubbles coalesce upon collision (Pilon et al., 2004). The first factor, frequency of collision in turn depends on the liquid flow and on the hydrodynamics interactions between the bubbles and the liquid phase.

Meanwhile the coalescence upon collision occurs when the collision duration time, t_c is larger than the time to drain the film between the bubbles, t_d . The probability of coalescence, P is expressed as a function of the collision duration time, t_c and the drainage time, t_d :

$$P = \exp(-t_d/t_c) \quad (1)$$

In the limiting cases, the thinning of the film separating two colliding bubbles is dominated by either viscous or inertial forces. The Weber number, a dimensionless expression is generally used in the studies of bubble coalescence. This expression represents the ratio of the inertial forces to the surface tension forces:

$$We = \frac{\rho V^2 r}{\sigma} \quad (2)$$

Where, ρ denotes liquid density, V the relative velocity of centers of colliding bubbles, r the bubble radius and σ the surface tension. Chesters (1991) has proposed an expression for each limiting cases by assuming that bubbles have the same radius and both gas viscosity and the van der Waals forces can be ignored:

$$\frac{t_d}{t_c} = \left(\frac{\rho V^2 r}{32\sigma} \right)^2 \quad \text{For inertia controlled drainage } (Re_{\infty} \leq 24) \quad (3)$$

$$\frac{t_d}{t_c} = \frac{3\mu}{\sqrt{2\sigma\rho r}} \quad \text{For viscosity controlled drainage } (Re_{\infty} > 24) \quad (4)$$

Another introduced term μ in the above equation denotes liquid viscosity. For inertia controlled drainage, increasing in the superficial gas velocity will increase the average bubble velocity while the probability of coalescence upon collision decreases. Otherwise, the probability of coalescence is independent of the superficial gas velocity. In addition, the size of the resultant bubble is determined by the type of coalescence, which in turn depends on the tubes spacing and the instance of bubble expansion at which coalescence occurs (N.A. Kazakis et al., 2008).

2.2 Bubble Transport

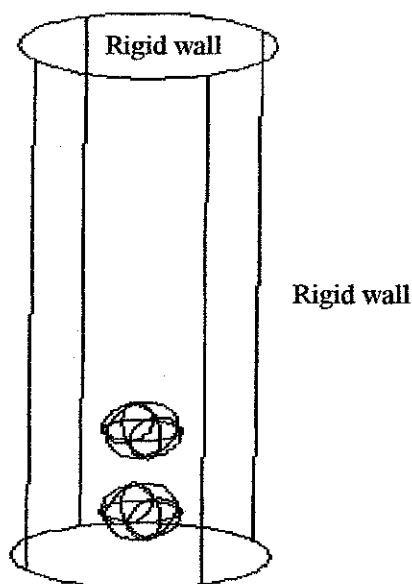


Figure 2.2: Schematic diagram of co-axial bubbles (Li Chen et al., 1998)

From Li Chen et al. (1998), the motion of the two bubbles can be described by the Navier-Stokes equation, which is written in a non-dimensional form as:

$$\nabla \cdot \mathbf{U} = 0 \quad (5)$$

$$\frac{\partial(\rho\mathbf{U})}{\partial t} + \nabla \cdot (\rho\mathbf{U} \otimes \mathbf{U}) = -\nabla p + \rho\mathbf{g} + \frac{1}{Re} \nabla \cdot [\mu(\nabla\mathbf{U} + \nabla\mathbf{U}^T)] + \frac{1}{Bo} \mathbf{F}_{sv} \quad (6)$$

with scales:

$$\begin{aligned} p^* &= \frac{p}{p_{ref}}; \mathbf{U}^* = \frac{\mathbf{U}}{u_{ref}}; x^* = \frac{x}{R_0}; \tau = \frac{t}{\tau_{ref}}; \\ \rho^* &= \frac{\rho}{\rho_{ref}}; \mu^* = \frac{\mu}{\mu_{ref}}; \sigma^* = \frac{\sigma}{\sigma_{ref}} \end{aligned} \quad (7)$$

in which:

$$u_{ref} = \sqrt{gR_0}; p_{ref} = \rho_{ref}u_{ref}^2. \quad (8)$$

Note that * is omitted in equations (5) and (6) for convenience. \otimes denotes the inner product of tensors, $\mathbf{U}(u_r, u_\theta, u_z)$ is the fluid velocity in $\mathbf{x}(r, \theta, z)$, ρ the density, μ the dynamic viscosity, p the pressure, $\mathbf{g}(0, 0, g)$ the gravity vector, R_0 initial bubble radius, and \mathbf{F}_{sv} the volume form of the surface tension force. The subscript, *ref*, stand for a reference value, and here, liquid properties are adopted as reference properties. Reynolds and Bond numbers are defined by:

$$Re = \frac{\rho_f g^{1/2} R_0^2}{\mu_{ref}}; Bo = \frac{\rho_f g R_0^2}{\sigma} \quad (9)$$

and

$$\begin{aligned} \rho(\mathbf{x}, t) &= F(\mathbf{x}, t)\rho_f + [1 - F(\mathbf{x}, t)]\rho_g; \\ \mu(\mathbf{x}, t) &= F(\mathbf{x}, t)\mu_f + [1 - F(\mathbf{x}, t)]\mu_g \end{aligned} \quad (10)$$

where F is the local volume fraction of one fluid. Its value may be unity in the liquid phase and zero in the gas phase if a gas-liquid two-phase system is involved. A value between 1 and 0 indicates a density interface. The last term of equation (6) is the surface tension force, which exists only at the interface and is modelled by the continuum surface tension force (CSF) method developed by Brackbill et al (1992). In this model, an interface is interpolated as a transient region with a finite thickness. Thus the surface tension force localised in this region can be converted into a volume force with the help of a Dirac delta function concentrated on the surface. The surface tension force is written as:

$$F_{sv} = \sigma \kappa(\mathbf{x}) \frac{\nabla \tilde{c}(\mathbf{x})}{[\tilde{c}]} \quad (11)$$

in which:

$$\kappa = -(\nabla \cdot \hat{\mathbf{n}}) \quad (12)$$

from the definition of a unit normal vector to a surface:

$$\hat{\mathbf{n}} = \frac{\nabla \tilde{c}}{|\nabla \tilde{c}|} \quad (13)$$

where \tilde{c} in the above equations is a colour function and $[\tilde{c}]$ is the difference of the colour function between two phases.

It is noted that Equations (9) and (10) represent discontinuous properties of fluid, which imply an interface between two-phase fluids, and they can be used to monitor the dynamics of the interface. However, when a large discontinuity is involved, for example a discontinuity of 850 in density ratio exists for a water-air system, numerical difficulties may arise in identifying an 'exact' interface. Thus, instead of solving the density transport equation directly, the volume fraction of liquid, F , is used to identify an interface. The transport of the F function is governed by:

$$\frac{\partial F}{\partial t} + \nabla \cdot (UF) = 0 \quad (14)$$

Also, the colour function, where \tilde{c} , in Equations (11) and (13) can be replaced by F . Now suitable initial and boundary conditions are required. In the case studied in this paper, an initially spherical gas bubble is located on the axis of a vertical cylinder filled with a stationary liquid. The boundary conditions are $\mathbf{U} = 0$ at the walls. The bubble is initially at rest.

2.3 Available Related Models

C.P. Ribeiro Jr and D. Mewes (2006) in their study have summarised the comparisons of models for film drainage that available in the literature which are in these models, the coalescence time is computed as the time required for the thin film of the continuous phase separating the interacting bubbles to drain from an initial thickness to a critical value, at which film rupture, and hence coalescence, occurs. A summary of the models available in the literature for pure liquids is given in Table 2.3.1.

Table 2.3.1: Available literature models for the coalescence time in pure liquids
(C.P. Ribeiro Jr., D. Mewes, 2006)

Reference	Main assumptions	Relations
Hodgson and Woods (1969)	Cylindrical drops; immobile interfaces; non-uniform film thickness; hydrostatic and inertia effects neglected; rupture at zero thickness; van der Waals forces included	$t_c = \frac{3\pi \eta_L r_b^{7/4}}{\sqrt{2} \sigma^{3/4} B^{1/4}}$
Chesters and Hofman (1982)	Spherical bubbles; mobile interfaces; non-uniform film thickness; inviscid, gravity-free fluid; uniform velocity across the film; van der Waals forces neglected	$t_c = \frac{\rho_L r_b^2 u_{rel}}{\sigma}$
Chen et al. (1984)	Spherical bubbles; immobile interfaces; non-uniform film thickness; inertia effects neglected; analysis of the rate of thinning at the rim of the film; van der Waals forces included; linear stability analysis used to predict critical film thickness for rupture	$t_c = 1.0704 \frac{\eta_L r_b^{17/5} [(\rho_L - \rho_G)g]^{3/5}}{\sigma^{6/5} B^{2/5}}$
Oolman and Blanch (1986)	Spherical bubbles; mobile interfaces; plane-parallel film; flat velocity profile in the film; van der Waals forces included; stagnant film at $t = 0$	$\frac{d^2\delta}{d\tau^2} = \frac{1.5}{\delta} \left(\frac{d\delta}{d\tau}\right)^2 - \alpha_1\delta - \frac{\alpha_2}{\delta^2}$ $\delta = \frac{h}{h_0}; \tau = \sqrt{\frac{\sigma\tau^2}{\rho_L h_0^3}}; \alpha_1 = \frac{8h_0^3}{r_b R_d^2}; \alpha_2 = \frac{2A}{3\pi\sigma R_d^2}$
Lee et al. (1987)	Spherical bubbles; partially immobile interfaces; plane parallel film; contributions of film thinning and rupture	$t_c = \min [t_1(h_c) + t_2(h_c)]$ $t_1(h_c) = -3M\eta_L R_d^2 \int_{h_0}^{h_c} \frac{dx}{8x^3 \left[\frac{2\sigma}{r_b} + \frac{A}{(6\pi x^3)} \right]}$ $t_2(h_c) = 24\pi^2 M\sigma\eta_L h_c^5 A^{-2}$
Jeelani and Hartland (1994)	Spherical bubbles; mobile interfaces; newtonian liquid film with uniform thickness; parabolic velocity profiles inside the bubbles	$t_c = \frac{3\pi\eta_L R_d^4}{4F h_c^2 \left[1 + \frac{3\eta_L r_b}{(\eta_G h_0)} \right]}$ $h_c = 0.267 \left(\frac{a_f A^2 r_b}{6\pi\sigma^2} \right)^{1/7}$
Li and Liu (1996)	Spherical bubbles; mobile interfaces; newtonian liquid film with non-uniform thickness; parabolic velocity profiles inside the bubbles; van der Waals forces included	$\frac{1}{\tau} = 40.0\beta^{0.46} + 141.49\beta^{0.26}\alpha^{1.02}$ $\tau = \frac{\sigma t_c h_0^3}{8\eta_L R_d^2}; \beta = \frac{R_d^2 B}{\sigma h_0^5}; \alpha = \frac{\eta_L}{2\eta_G R_d} (r_{b,1} + r_{b,2})$

Meanwhile, Ryszard Pohorecki et al. (2001) has summarised the different correlations for the influence of liquid properties on the average bubble diameter as shown in Table 2.3.2.

Table 2.3.2: Influence of liquid properties on the bubble diameter
(Ryszard Pohorecki et al., 2001)

Correlation	Liquid Density	Liquid Viscosity	Surface Tension
Hughmark (1967)	$\rho_L^{-0.2}$	μ_L^0	$\sigma^{0.6}$
Van Dierendonck (1970)	$\rho_L^{-0.5}$	μ_L^0	$\sigma^{0.5}$
Akita and Yoshida (1974)	$\rho_L^{-0.74}$	$\mu_L^{0.24}$	$\sigma^{0.5}$
Kumar, Degaleesan, Laddha, and Hoelscher (1976)	$\rho_L^{-0.25}$	μ_L^0	$\sigma^{0.25}$
Idogawa, Ikeda, Fukuda, and Morooka (1986)	ρ_L^0	μ_L^0	$\sigma^{0.08^a}; \sigma^{0.03^b}$
Idogawa, Ikeda, Fukuda, and Morooka (1986)	ρ_L^0	μ_L^0	$\sigma^{0.20^a}; \sigma^{0.08^b}$
Wilkinson (1991)	$\rho_L^{-0.45}$	$\mu_L^{0.22}$	$\sigma^{0.6}$

^a $p = 0.1 \text{ MPa}$; ^b $p = 1.0 \text{ MPa}$

2.4 Computational Fluid Dynamics

Computational fluid dynamics (CFD) is one of the branches of fluid mechanics that uses numerical methods and algorithms to solve and analyze problems that involve fluid flows. CFD offers a qualitative prediction of fluid flows by means of mathematical modeling, numerical methods and software tools (Dmitri Kuzmin). Numerical solutions provided by CFD have allowed the analysis of complex phenomena without having to invest in complicated experimental measurement and expensive prototype (Fadlun, Verzicco et al., 2000). The most basic consideration in CFD is how to treat a continuous fluid in a discretized fashion on a computer. One of the methods is to discretize the spatial domain into small cells to form a volume mesh or grid. Next a suitable algorithm is applied to solve the equations of motion which either Euler equations for inviscid or Navier-Stokes equations for viscous flow.

At two-phase flow point of view, the modeling is still under development and different methods have been proposed in the flow analysis. Numerically, a robust algorithm with an accurate representation of interfaces is needed to handle the complex topological changes during the bubble fusion. In former literature, Volume-tracking

methods that account for the interface in an implicit way such as Volume-of-Fluid (VOF) or Level Set method are in principle suitable to represent the coalescence process. Most of these methods are either good in maintaining a sharp interface or at conserving mass. This is important as the evaluation of the density, viscosity and surface tension is based on the values averaged over the interface.

VOF method is commonly used as the numerical method for the dynamics and deformation for the liquid-air interface (J.M. Martinez et al.). In fact, this method is widely used for two phase flow simulations and shows a good agreement between numerical and experimental data. This technique is applied for tracking and locating the free surface or fluid-fluid interface. The VOF is an Eulerian fixed-grid technique and it belongs to the class of Eulerian methods which are characterized by a mesh whether is stationary or is moving in a certain prescribed manner to accommodate the evolving shape of the interface. Besides, the VOF method is known for its ability to conserve the mass of the traced fluid and also it can trace easily the topology changes by fluid interface. In spite of this, a disadvantage on VOF method is the so-called artificial coalescence of gas bubbles which happens when their mutual distances is less than the size of the computational cell (Deen, Annaland et al., 2009). Furthermore VOF model however is inappropriate if bubbles are small compared to a control volume, namely bubble column (André Bakker, 2002).

Recently, the nonstop development of computational power has been one on the driving force that encourages the usage of CFD for engineers. As forming a new trend in finding technological solutions, fluid dynamics simulations have raised some main issues which are accuracy, computational efficiency and the ability to handle complex geometries. A real challenge in CFD comes when dealing with complex fluid flow analysis. The simulation of a flow around a realistic configuration is extremely complex since the shape of the domain must include wetted surface of the geometry of interest (Iaccarino and Verzicco, 2003). Another factor that complicates the analysis when geometry complexity is combined with moving boundaries and high Reynolds numbers in which significantly increase the computational difficulties; since they require

regeneration or deformation of the grid and turbulence modelling (Fadlun, Verzicco et al., 2000).

Looking for a recent advanced alternative in dealing with complex fluid flow analysis, the Immersed Boundary (IB) technique is introduced nowadays. This technique allows the solution of differential equations in complex geometric configurations on simple meshes by introducing forcing conditions on certain surfaces corresponding to the physical location of the complex boundaries (Iaccarino and Verzicco, 2003). This method is applied in such a way the bodies of almost arbitrary shape can be added without altering the computational grid, that considerably avoid a time-consuming process (Yusof, 1998).

2.5 Volume-of-Fluid (VOF) Model

The VOF is formulated in principle that two or more phases are not interpreting. In fact, for each additional phase added to the model, a variable is introduced which is the volume fraction of the phase in the computational cell (Fluent Manual, 2003). In each control volume, the volume fractions of all phases sum to unity. As long the volume fraction of each phase is known at each location, the fields and properties are shared by phases and being represented as volume-averaged values. If the q-th fluid's volume fraction is denoted as a α_q hence three conditions are possible happened within a cell:

- a) $\alpha_q = 0$; the cell is empty (of the q-th fluid)
- b) $\alpha_q = 1$: the cell is full (of the q-th fluid)
- c) $0 < \alpha_q < 1$; the cell contains the interface between the q-th fluid with one or more others fluid

The tracking of the interface(s) between the phases is generated by the solution of continuity equation for the volume fraction of one (or more) of the phases.

$$\frac{\partial \alpha_q}{\partial t} + \vec{v} \cdot \nabla \alpha_q = \frac{S \alpha_q}{\rho_q} \quad (15)$$

The volume fraction equation will not be solved for the primary phase due to the constraint as following:

$$\sum_{q=0}^n \alpha_q = 1 \quad (16)$$

The properties appearing in the transport equations are determined by the presence of the component phases in each control volume. Generally the volume-fraction-averaged density for an n-phase system can be expressed as equation 7. All other properties also take on the following form to be computed.

$$\rho = \sum \alpha_q \rho_q \quad (17)$$

In VOF model, a single momentum equation used to solve throughout the domain and the resulting velocity is shared among the phases. The momentum equation is dependent on the volume fractions of all phases via the properties ρ and μ . However shared-fields approximation has one limitation when a large velocity differences exist between the phases. The accuracy of the velocities computed near the interface can be adversely affected. The momentum equation is shown below:

$$\frac{\partial t}{\partial} (\rho \vec{v}) + \nabla \cdot (\rho \vec{v} \vec{v}) = -\nabla p + \nabla \cdot [\mu (\nabla \vec{v} + \nabla \vec{v}^T)] + \rho \vec{g} + \vec{F} \quad (18)$$

The energy equation also shared among the phases and the VOF model treats energy, E and temperature, T , as mass-averaged variables respectively shown below:

$$\frac{\partial}{\partial t} (\rho E) + \nabla \cdot (\vec{v} (\rho E + p)) = \nabla \cdot (k_{eff} \nabla T) + S_h \quad (19)$$

$$E = \frac{\sum_{q=1}^n \alpha_q \rho_q E_q}{\sum_{q=1}^n \alpha_q \rho_q} \quad (20)$$

In the above equation E_q for each phase is based on the specific heat of that phase and the shared temperature. The properties ρ and thermal conductivity, k_{eff} are shared by the phases. Meanwhile the source term, S_h contains contributions from radiation, as well as any other volumetric heat sources.

2.6 Modelling Case Overview

A case has been selected for modelling case which is taken from Li Chen et al. (1998), entitled “The Coalescence of Bubbles – A Numerical Study”. A literature review on the selected case is performed as below:

The team has studied the dynamics of bubble coalescence using a robust numerical model for a multiphase flow system with interfaces. In their research, they also investigated the effects of liquid viscosity and surface tension on bubble coalescence, for which Reynolds number ranges from 10 to 100 and Bond number ranges from 5 to 50.

In order to validate the numerical solution, Li Chen et al. (1998) had carried out an experiment with a glycerin liquid with $\rho_f \approx 1220 \text{ kg/m}^3$, $\mu_f = 0.11 \text{ kg/m.s}$, and $\sigma = 0.006 \text{ N/m}$. The experimental procedure is taken from Manasseh et al. (1998) where the air bubbles were produced from compressed and filtered air in pressure-controlled mode. The underwater nozzle had internal diameter of 6.0 mm and it was machined to maintain its internal edge as sharp as possible in ensuring a known contact radius of bubbles. The nozzle orifice was at depth of 0.23 m. The schematic diagram of apparatus is shown from Figure 2.6.1.

Meanwhile, the equivalent radius of a spherical bubble was determined from the acoustic frequency of bubble oscillation Manasseh (1997). These properties give equivalent non-dimensional parameters which are $Bo=5$, $M=4.1 \times 10^{-3}$ and $\rho_f/\rho_g \approx 1000$ with a 10% error in both density and viscosity estimation. The similarity of the bubble coalescence between the predicted and experimental results can be seen from Figures 2.6.2 and 2.6.3.

From both methods, the experimental result for the average rise velocity, with reference to the leading bubble centre before coalescence, gives 0.3 ms^{-1} , while the numerical simulation gives 0.24 ms^{-1} . The validation gives an error of 20%. Based on

Figures 2.6.2 and 2.6.3, it is observed that the differences between the numerical and experimental following bubbles appear mostly in the first two frames. This happens due to the different initial conditions. However, the agreement between the results may be considered reasonable, given the somewhat different initialization and uncertain fluid properties in the experiment.

From the validation, it is shown that the numerical model used in this study can accurately capture the complex topological changes during the coalescence. The predicted behavior of bubble coalescence is in reasonable agreement with the experimental result. It is also found in this paper that with a high Reynolds number (low viscosity) a strong liquid jet formed behind the leading bubble inhibits the approach of the following bubble. Thus coalescence does not occur or is postponed. The effect of surface tension on bubble coalescence shows that; a lower surface tension results in an earlier coalescence because of severe stretching of the interface.

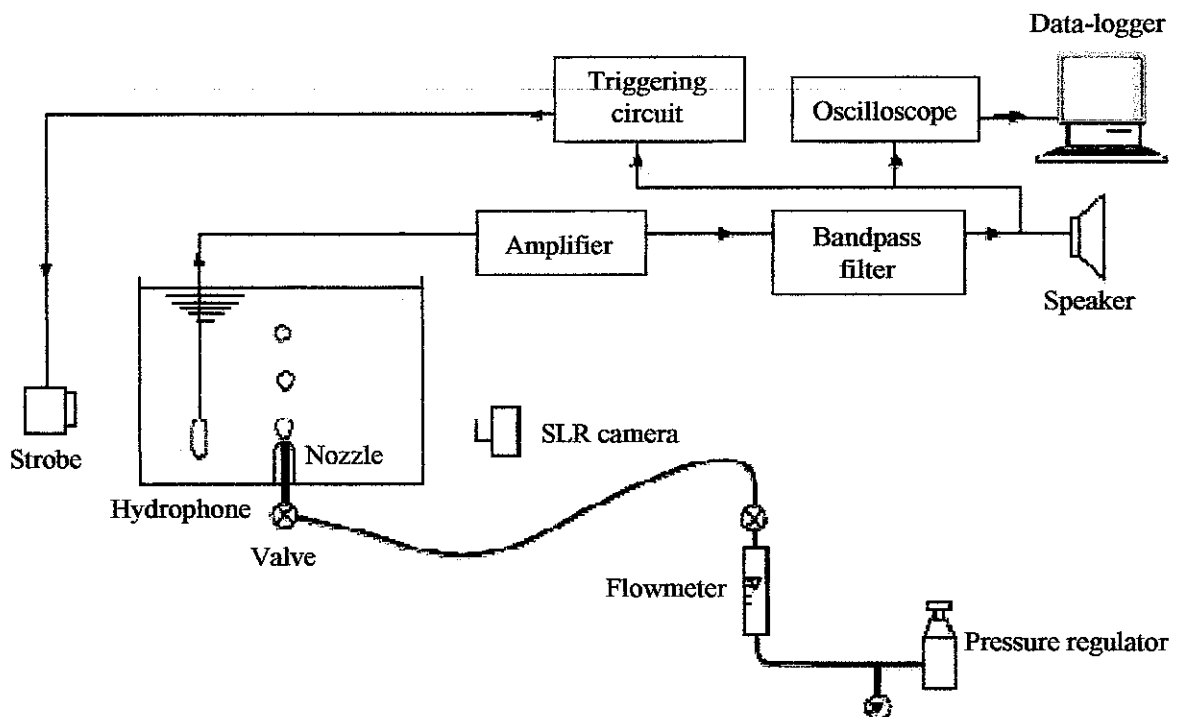


Figure 2.6.1: Schematic diagram of apparatus
(Manasseh et al., 1998)

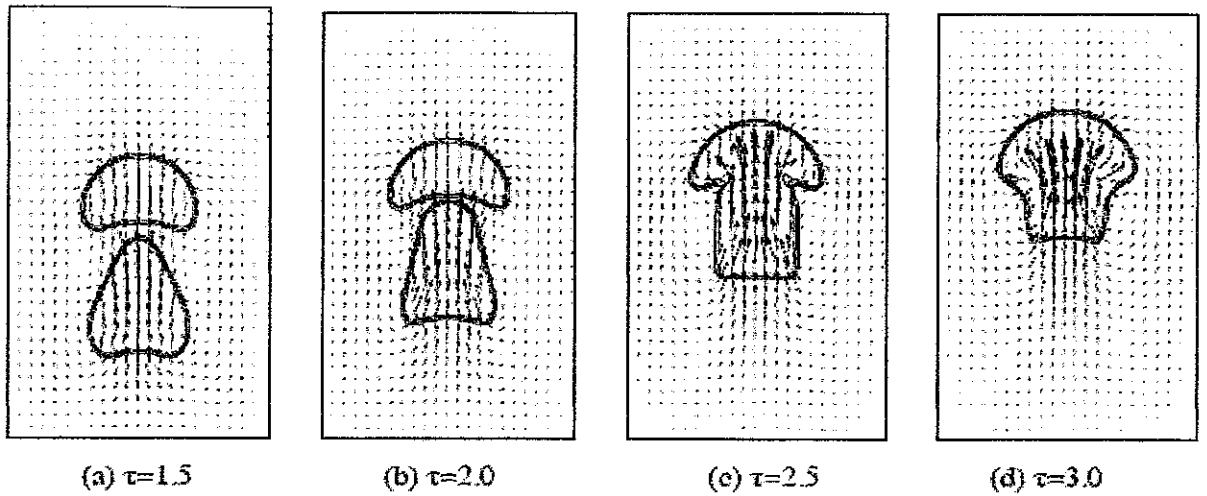


Figure 2.6.2: Predicted axisymmetric coalescence of two gas bubbles in a viscous liquid
 ($Re=12$, $Bo=5$, $M=4.1 \times 10^{-3}$, $\rho_f/\rho_g=1000$, $\mu_f/\mu_g=100$, $z/R_0=0.36$)
 (Li Chen et al., 1998)

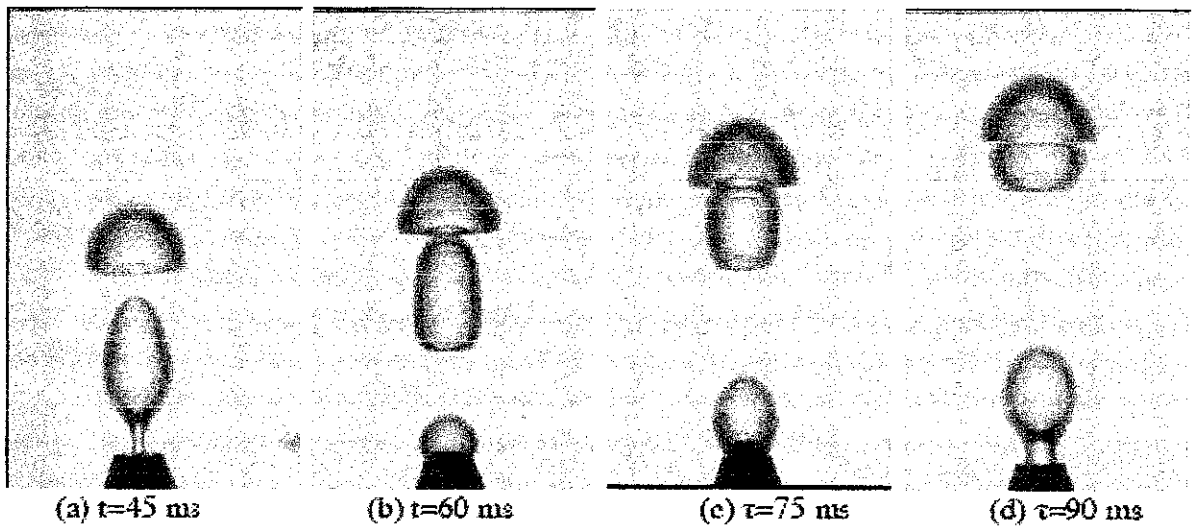


Figure 2.6.3: Experimental observation of the axisymmetric coalescence of two gas
 bubbles in a glycerin liquid
 ($M=4.1 \times 10^{-3}$, $Bo=5$, $\rho_f/\rho_g \approx 1000$)
 (Li Chen et al., 1998)

CHAPTER 3

METHODOLOGY / PROJECT WORK

3.1 Project Flow Chart

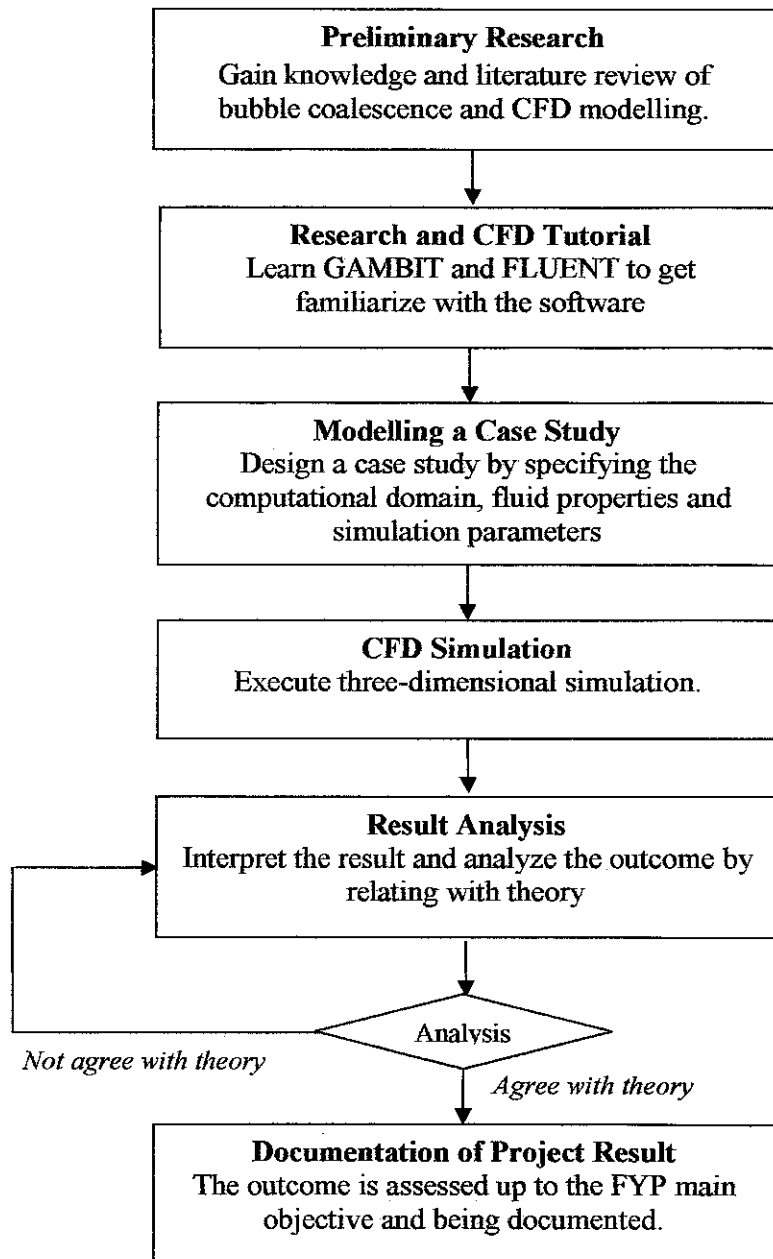


Figure 3.1: Project flow chart

3.2 Project Work Execution

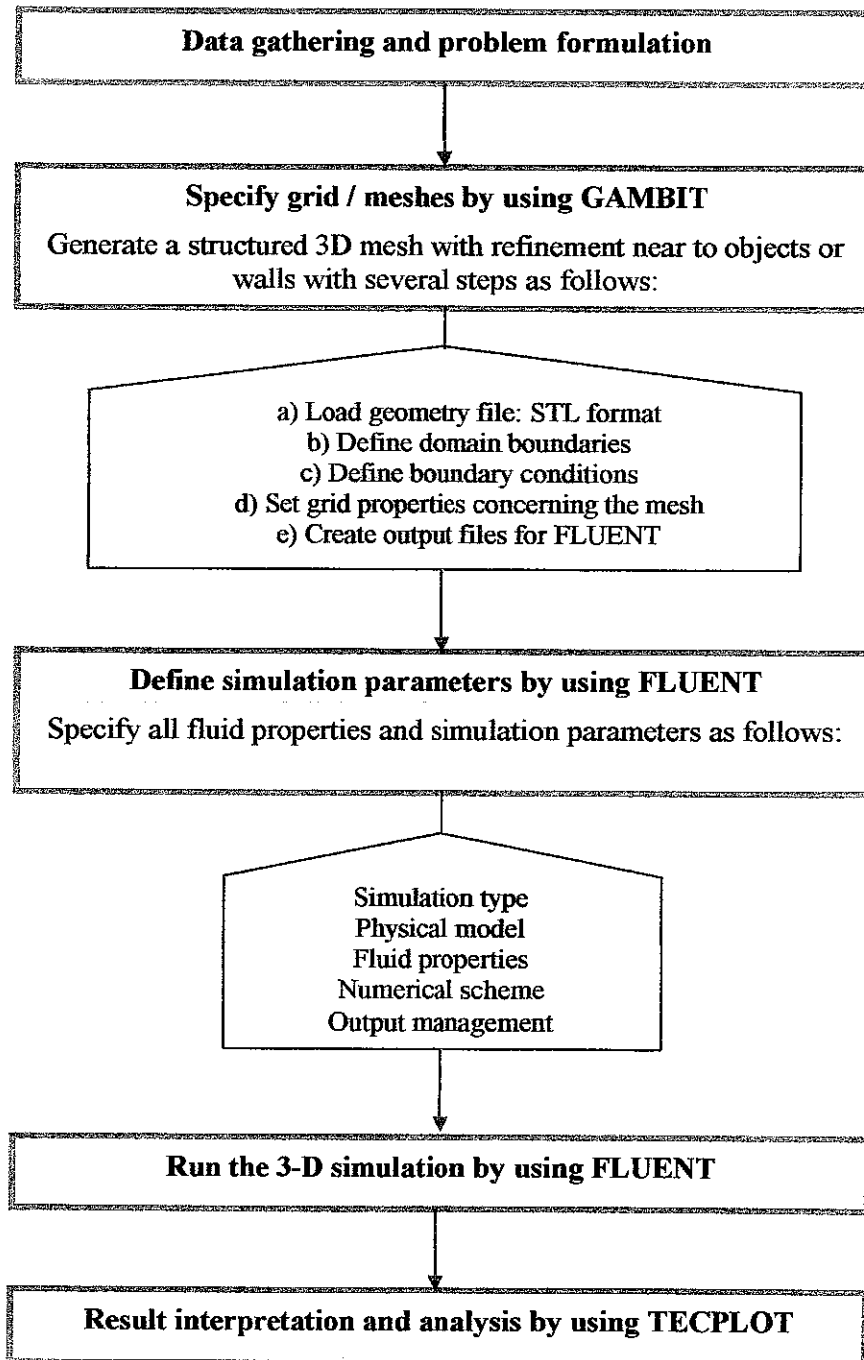


Figure 3.2: Project work execution

3.3 Project Gantt Chart

No.	Detail/ Week	1	2	3	4	5	6	7	8	9	10	11	12	13	14
1	Selection of project topic	■	■												
2	Preliminary research		■	■	■	■									
3	Submission of preliminary report					●									
4	Project work starts				■	■	■	■	■						
5	Submission of progress report									●					
6	Seminar										●				
7	Project work continues										■	■	■	■	
8	Submission of interim report													●	
9	Oral presentation														●

Figure 3.3.1: Gantt chart of FYP 1

No.	Detail/ Week	1	2	3	4	5	6	7	8	9	10	11	12	13	14	15	16	17	18	19
1	Project work continues	■	■	■																
2	Submission of progress report 1					●														
3	Project work continues				■	■	■	■	■											
4	Submission of progress report 2										●									
5	Project work continues										■	■	■							
6	Poster exhibition											●								
7	Submission of dissertation report (soft bound)													●						
8	Oral presentation																	●		
9	Submission of dissertation report (hard bound)																			●

Figure 3.3.2: Gantt chart of FYP 2

Legend:	●	Milestone	■	Activities
---------	---	-----------	---	------------

3.4 Tools and Equipment

The main tool required in this Bubble-Bubble Coalescence Project is Computational Fluid Dynamics software. The simulation is handled with a systematic procedure shown in Figure 3.2. However for all CFD software, a basic procedure applied. Briefly, during pre-processing, the geometry of the problem is first defined. The volume occupied by the fluid is then divided into mesh. After that, the physical modelling, boundary conditions and fluid properties are further specified. The simulation is started and the equations are solved iteratively. Lastly the result is analyzed by using a processor.

In this project, the simulation will use FLUENT as the software to study the dynamics of coalescence phenomenon. GAMBIT is used to draw and mesh the 3-D computational domain for the problem. The simulation will be done to study the behaviour of bubble coalescence and effect of certain model parameters on the bubble properties. Other tools used are TECPLOT for post-processing and AutoCAD for technical drawing purpose.

CHAPTER 4

RESULTS AND DISCUSSION

4.1 The Behavior of Bubble Coalescence

4.1.1 Modelling

In modelling the framework, several assumptions have been specified to the system (as stated in the scope of study):

- Laminar and low Reynolds number of flow
- Liquid and gas are isothermal and incompressible
- Two co-axial bubbles with the identical radius rising in line
- Bubble is free rising under gravity presence
- Cylindrical tank is used

The fluid selected into this case is water (liquid) and oil (bubbles). With these fluid properties of water-oil system, calculation had been done in order to obtain some value of parameters, namely bubble radius, and velocity of the bubbles.

a) Bubble radius, r_b

In this modelling, the bubble radius is calculated by using the correlation given by Minnaert (1933). Minnaert (1933) has found the fundamental relation between bubble acoustic frequency and radius by equating the potential energy of the compressed gas at one node of the oscillation cycle, with the kinetic energy of the fluid set in motion around the bubble at the antinode:

$$2\pi f = \sqrt{\frac{3\gamma P_0}{\rho_f r_b^3}} \quad (21)$$

where the values are:

$$f = \text{frequency}$$

$$f = 0.95 \pm 0.002 \text{ kHz} = 950/s$$

→ acoustic frequency from the first period of oscillation, Manasseh (1998)

$\rho_f = \text{liquid density}$

$$\rho_f = 997 \text{ kg/m}^3$$

$P_0 = \text{absolute liquid pressure}$

$$P_0 = P_{atm} + \rho_f gh$$

$$P_0 = \left(\frac{1.01325 \times 10^5 \text{ kg}}{\text{ms}^2} \right) + \left(\frac{997 \text{ kg}}{\text{m}^3} \right) \left(\frac{9.81 \text{ m}}{\text{s}^2} \right) (0.23 \text{ m})$$

$$P_0 = 103574.5 \text{ kg/ms}^2$$

$\gamma = \text{ratio of specify heats for the gas (air)}$

$$\gamma = 1.401$$

→ at temperature 20°C, refer APPENDIX A.

substituting the values into equation (21):

$$2\pi \left(\frac{950}{\text{s}} \right) = \sqrt{\frac{3(1.401) \left(\frac{103574.5 \text{ kg}}{\text{ms}^2} \right)}{\left(\frac{997 \text{ kg}}{\text{m}^3} \right) r_b^2}}$$

$$r_b = 0.0031723 \text{ m} = 0.00317 \text{ m} = 3.17 \text{ mm.}$$

From Manasseh et al. (1998) study, the larger bubbles of 2-4 mm radius were examine since these are of greater industrial relevance and also permits closer visualisation of the bubble dynamics. Meanwhile, the bubble radius obtained from the calculation is 3.17 mm which lies in the range between 2-4 mm of radius, thus the value is considered to be reasonable.

b) Velocity of bubble, v_b

The velocity of the bubble can be estimated from equation (22):

$$v_b = \frac{\left(\frac{2}{9} \right) (\tau_b^2) \rho_f g}{\mu_f} \quad (22)$$

where other values are:

$g = \text{gravity}$

$$g = 9.81 \text{ m/s}^2$$

$\mu_f = \text{viscosity}$

$$\mu_f = 1.04 \times 10^{-3} \text{ kg/ms}$$

substituting the values into equation (22):

$$v_b = \frac{\left(\frac{2}{9}\right) (0.00317 \text{ m})^2 \left(\frac{997 \text{ kg}}{\text{m}^3}\right) \left(\frac{9.81 \text{ m}}{\text{s}^2}\right)}{\left(\frac{1.04 \times 10^{-3} \text{ kg}}{\text{ms}}\right)}$$

$$v_b = 21.001 \text{ m/s}$$

c) Initial distance between successive bubbles, S

An assumption has been done in order to specify the spacing between the bubbles as following:

$$S = 3r_b \tag{23}$$

substituting the obtained value of r_b into equation (23):

$$S = 3(3.17 \text{ mm}) = 9.51 \text{ mm}$$

Note that D is the distance from the bubble centre to another bubble centre.

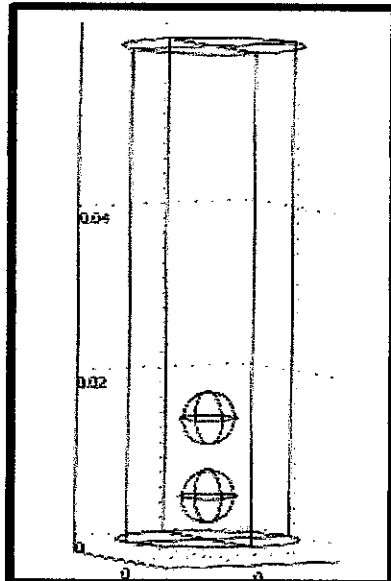


Figure 4.1.1: Computational domain

The boundary conditions and the relevant parameters of the case study have been tabulated in Table 4.1.

Table 4.1: Boundary conditions and fluid properties

Grid / boundary conditions		
Tank domain	Cylinder with r=10 mm, h=60 mm	
Boundary conditions	All boundaries are wall.	
Refinement method	Refine blocks	
Spacing	9.51 mm (spacing between bubbles centre)	
Bubble size	Two bubbles with radius of 3.17 mm	
Bubble location	Two bubbles are aligned in the centre of the cylindrical domain with different height: h ₁ = 5.17 mm h ₂ = 14.68 mm	
Fluid properties / simulation parameters		
Simulation parameters	Simulation model	Volume-of-Fluid (VOF)
	Simulation type	Unsteady, implicit
Fluid properties	Phase 1 (Bubbles)	Oil
	Density	800 kg/m ³
	Viscosity	0.00168 kg/m.s
	Phase 2 (Liquid)	Water
	Density	997 kg/m ³
	Viscosity	1.04 × 10 ⁻³ kg/m.s
	Surface tension	0.023 N/m
Operating conditions	Operating pressure	101.325 kPa
	Operating density	800 kg/m ³ (density of oil)
	Gravity acceleration	9.81 m/s ²

4.1.2 Result and Discussion

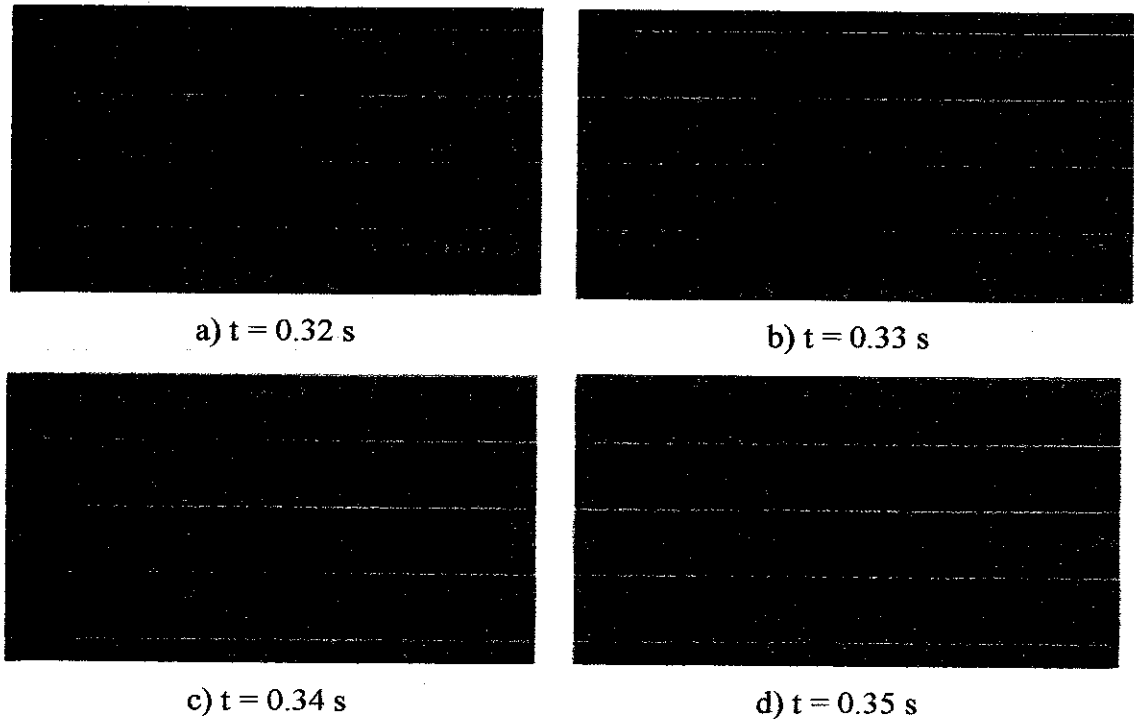


Figure 4.1.2: Series of contours of volume fraction

Figure 4.1.2 shows the some relevant plots of contours of volume fraction during bubble coalescence process of two bubbles. The behaviour of bubble coalescence is investigated. At initial condition $t = 0$ s, the two spherical bubbles were stationary and when simulation began, the bubbles were observed to start rising due to the buoyancy force. As time progresses, the two spherical bubbles became ellipsoids in shape due to pressure difference between the top and bottom surfaces of the bubbles. Based on Figure 4.1.2 a, the liquid circulation around the bubble produced a jet to push in the lower surface of both leading and following bubbles and the deformations of the bubbles occur. The pressure, behind the leading bubble controlled the entrainment of the following bubble by promoting a slight acceleration and elongation of the following bubble which eventually causes the coalescence to occur (Li Chen et al., 1998).

As the bubbles started approaching each other at $t = 0.34$ ms (Figure 4.1.2 c), the following bubbles accelerates and then collided. Upon collision impact, there is

flattening of the bubbles surfaces in contact, leaving a thin liquid film separating them (Figure 4.1.2 d). Coalescence will take place if the two bubbles stay in contact for longer than is required for the film to thin (Oolman, T. O. and Blanch, H. W., 1986). Once the film is sufficiently thin, an instability mechanism will result in film rupture and formation of a coalesced bubble.

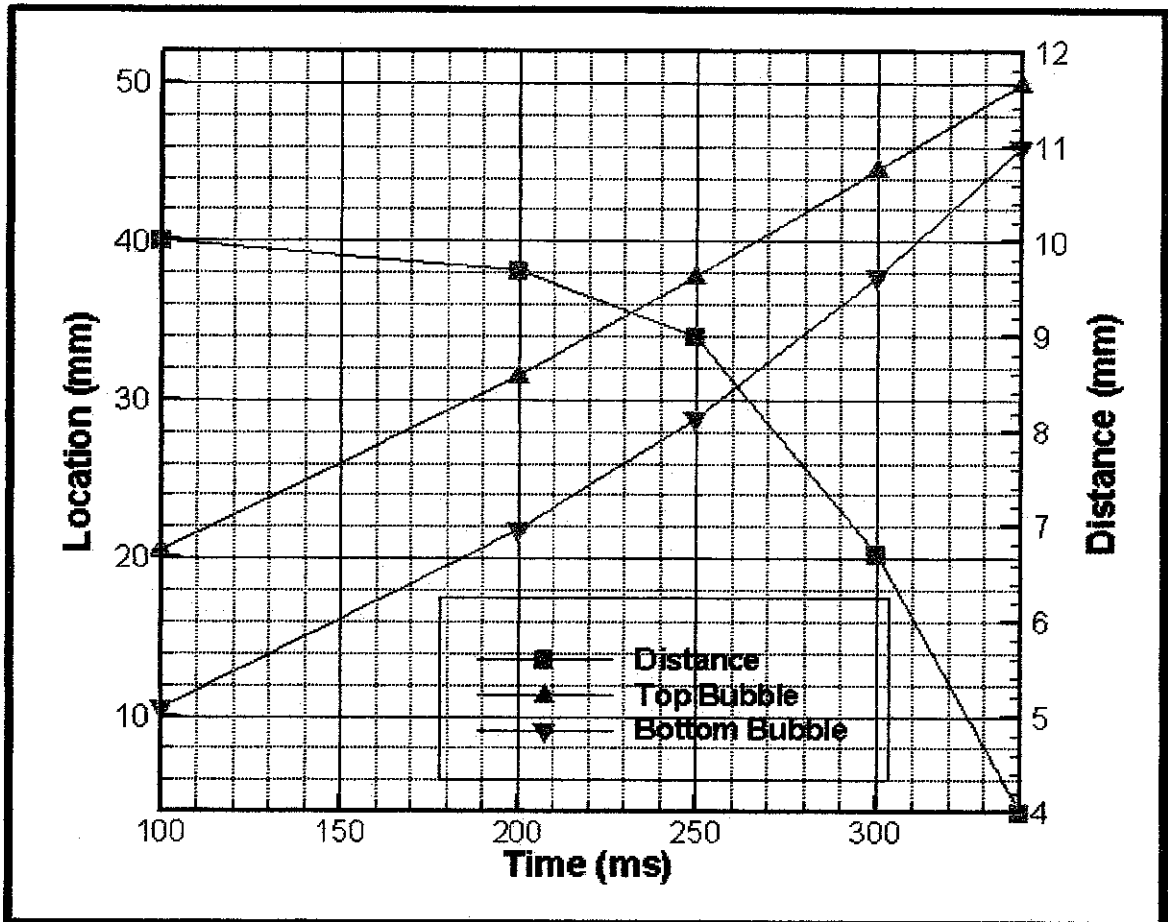


Figure 4.1.3: Position of two bubbles as a function of time

The bubble trajectories are plotted as shown in Figure 4.1.3. Based on the figure, it is observed that the bubbles which are top and the bottom bubbles start to rise and approach each other as the time progresses. The distance between the two bubbles is getting smaller until it coalesced estimated at $t = 0.35$ s.

4.2 The Effect of Surface Tension on Bubble Coalescence

4.2.1 Modelling

A case has been selected for validation which is taken from Li Chen et al. (1998), entitled "The Coalescence of Bubbles – A Numerical Study". The literature review on the selected case can be referred to previous Section 2.6. To start modelling, the bubble radius is calculated from the parameters given. In the validation, the values of time is represented in dimensionless time, τ . Thus we also need to calculate the value of reference time, t_{ref} in our calculation in order to obtain the real time values, t_{real} . The related calculations are shown as below:

Given the parameters as follows:

$$\rho_f = 1220 \text{ kg/m}^3$$

$$\mu_f = 1.7894 \times 10^{-3} \text{ kg/m.s}$$

$$\sigma = 0.066 \text{ N/m} = 0.066 \text{ kg/s}^2$$

$$Re = 10$$

$$Bo = 5$$

as the relative ratio of density and viscosity are given by:

$$\rho_f / \rho_g = 850 \text{ and } \mu_f / \mu_g = 100$$

therefore:

$$\rho_g = 1.435 \text{ kg/m}^3$$

$$\mu_g = 1.7894 \times 10^{-5} \text{ kg/m.s}$$

a) Bubble radius, R_b

In this modelling, the bubble radius is calculated by using the dimensionless correlation as follows:

$$\text{Reynolds number} = Re = \frac{Dv\rho}{\mu} = \frac{R_b(gR_b)^{0.5}\rho_f}{\mu_f} \quad (24)$$

substituting the values into equation (24):

$$Re = \frac{R_b (gR_b)^{0.5} \rho_f}{\mu_f} = \frac{\left(\frac{9.81 \text{ m}}{\text{s}^2}\right)^{0.5} \left(\frac{1220 \text{ kg}}{\text{m}^3}\right) R_b^{1.5}}{\left(\frac{1.7894 \times 10^{-3} \text{ kg}}{\text{m/s}}\right)}$$

$$R_b = 2.799 \times 10^{-4} \text{ m}$$

b) Relative velocity, u_{rel}

Relative velocity can be computed from this formula as follows:

$$u_{rel} = \sqrt{gR_b} \quad (25)$$

substituting the values into equation (25):

$$u_{rel} = \sqrt{\left(\frac{9.81 \text{ m}}{\text{s}^2}\right) (2.799 \times 10^{-4} \text{ m})}$$

$$u_{rel} = 0.0524 \text{ m/s}$$

c) Reference time, t_{ref}

Reference time can be computed from this formula as follows:

$$t_{ref} = \frac{R_b}{u_{rel}} \quad (26)$$

substituting the values into equation (26):

$$t_{ref} = \frac{2.799 \times 10^{-4} \text{ m}}{0.0524 \text{ m/s}}$$

$$t_{ref} = 5.342 \times 10^{-3} \text{ s} = 5.342 \text{ ms}$$

d) Real time, t_{real}

The dimensionless time is given by this formula:

$$\tau = \frac{t_{real}}{t_{ref}} \quad (27)$$

For example of calculation, real time, t_{real} at dimensionless time of $\tau=0.5$ can be computed as follow:

$$t_{real} = \tau \times t_{ref} = 0.5 \times (5.342 \times 10^{-3} \text{ s}) = 2.671 \times 10^{-3} \text{ s}$$

The values of t_{real} are computed for several values of τ ranging from 0.5 to 3 as shown in table below. The position of two bubble centres as a function of time will be read at t_{real} from the simulation.

Table 4.2.1: Real time data

τ	0.5	1.0	1.5	2.0	2.5	3.0
t_{real} (s)	0.002671	0.005342	0.008013	0.010684	0.013355	0.016026

e) Tank dimension

The tank used is cylindrical with the dimension is assumed as follows:

$$Tank\ radius = R_t = 10R_b \tag{28}$$

$$Tank\ height = H_t = 40R_b \tag{29}$$

substituting the obtained value of R_b into equation (28) and (29):

$$R_t = 10(2.799 \times 10^{-4} m) = 2.799 \times 10^{-3} m$$

$$H_t = 40(2.799 \times 10^{-4} m) = 0.011196 m$$

f) Initial distance between successive bubbles, S

An assumption has been done in order to specify the spacing between the bubbles as following:

$$S = 2.36R_b \tag{30}$$

substituting the obtained value of R_b into equation (30):

$$S = 2.36(2.799 \times 10^{-4} m) = 6.606 \times 10^{-4} m$$

where S is the distance from the bubble centre to another bubble centre.

g) Bubbles location

Two bubbles are initially aligned in the centre of the cylindrical tank with different height, h_1 for bottom (following) bubble and h_2 for top (leading) bubble:

$$h_1 = 4R_b \tag{31}$$

$$h_2 = h_1 + S \quad (32)$$

substituting the values into equation (31) and (32):

$$h_1 = 4(2.799 \times 10^{-4} \text{ m}) = 1.1196 \times 10^{-3} \text{ m}$$

$$h_2 = (1.1196 \times 10^{-3} \text{ m}) + (6.606 \times 10^{-4} \text{ m}) = 1.7802 \times 10^{-3} \text{ m}$$

where h_1 and h_2 are measured from the tank bottom to the each bubble centre respectively. The data calculated are tabulated in Table 4.2.2. The sketch and illustration of computational domain with the specified dimension is shown in Figure 4.2.1.

Table 4.2.2: Boundary conditions and fluid properties

Grid / boundary conditions			
Tank domain	Cylinder with $R_t = 2.799 \times 10^{-3} \text{ m}$, $H_t = 0.011196 \text{ m}$		
Boundary conditions	All boundaries are wall.		
Refinement method	Refine blocks		
Spacing, S	$6.606 \times 10^{-4} \text{ m}$ (spacing between bubbles centre)		
Bubble radius, R_b	$2.799 \times 10^{-4} \text{ m}$		
Bubble location	$h_1 = 1.1196 \times 10^{-3} \text{ m}$, $h_2 = 1.7802 \times 10^{-3} \text{ m}$		
Fluid properties / simulation parameters			
Simulation parameters	Simulation model		Volume-of-Fluid (VOF)
	Simulation type		Unsteady, implicit
Fluid properties	Phase 1 (Bubbles)	Density, ρ_g	1.435 kg/m^3
		Viscosity, μ_g	$1.7894 \times 10^{-5} \text{ kg/m.s}$
	Phase 2 (Liquid)	Density, ρ_f	1220 kg/m^3
		Viscosity, μ_f	$1.7894 \times 10^{-3} \text{ kg/m.s}$
	Surface tension, σ		$0.066 \text{ N/m} = 0.066 \text{ kg/s}^2$
Operating conditions	Operating pressure		101.325 kPa
	Operating density		1.435 kg/m^3 (density of bubbles)
	Gravity acceleration		9.81 m/s^2

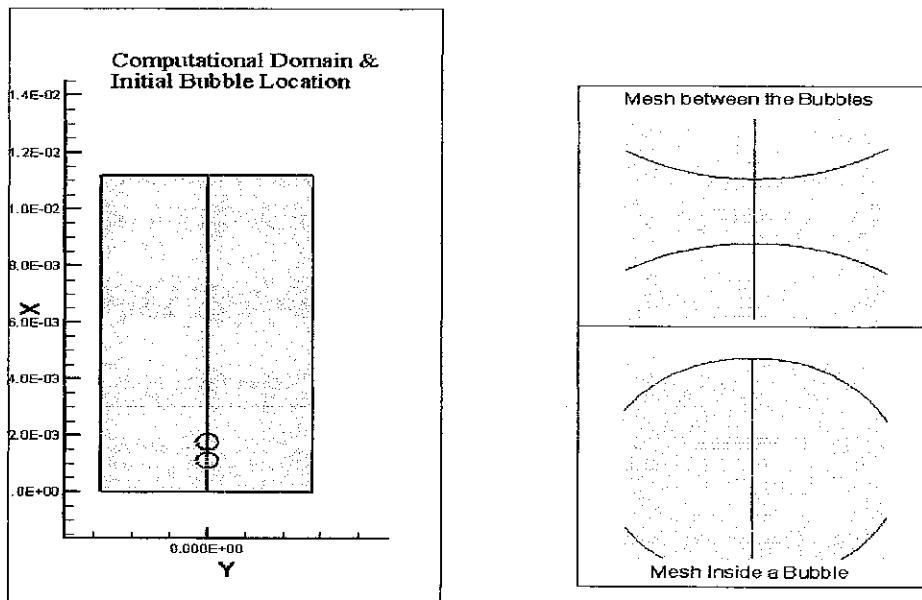
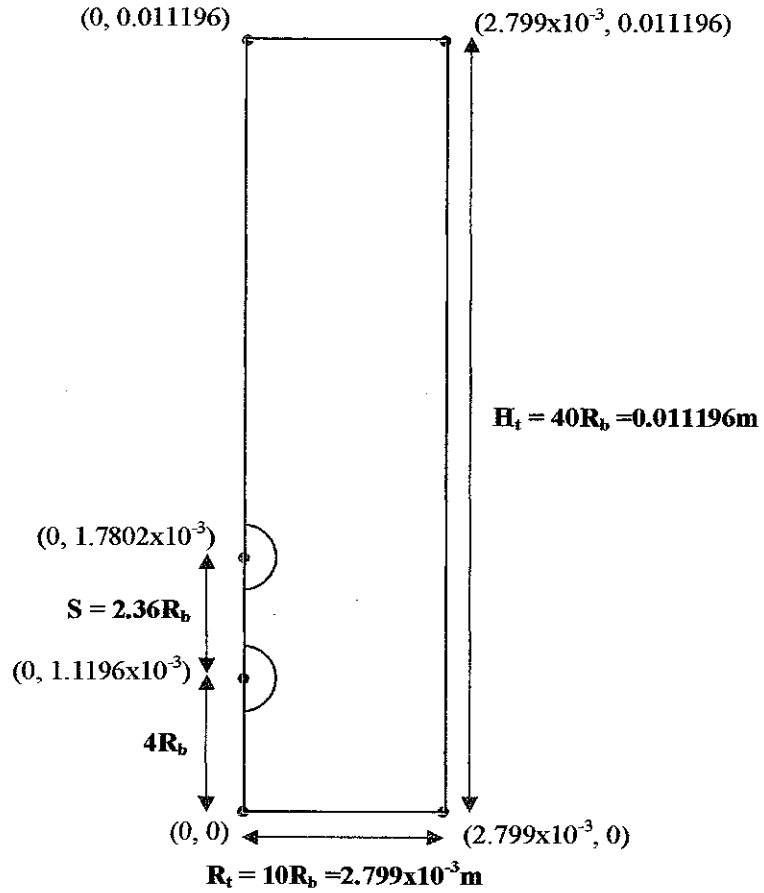


Figure 4.2.1: Computational domain

By using constant parameter of bubble radius, $R_b = 2.799 \times 10^{-4}$ m, another two test cases also be performed to study the effect of surface tension on bubble coalescence. The original case (Case 1) and other 2 cases' parameters have been tabulated at different values of Re and Bo number as shown in Table 4.2.3. The Re and Bo are changed by manipulating the value of liquid density and surface tension respectively; while other values like viscosities, density ratio and viscosity ratio are kept constant.

Table 4.2.3: Parameters for simulation test cases

Test Case	Reynolds number (Re)	Bond number (Bo)	Density ratio (ρ_f/ρ_g)	Viscosity ratio (μ_f/μ_g)
1	10	5	850	100
2	10	50	850	100
3	8.5	4.25	850	100

4.2.2 Result and Discussion

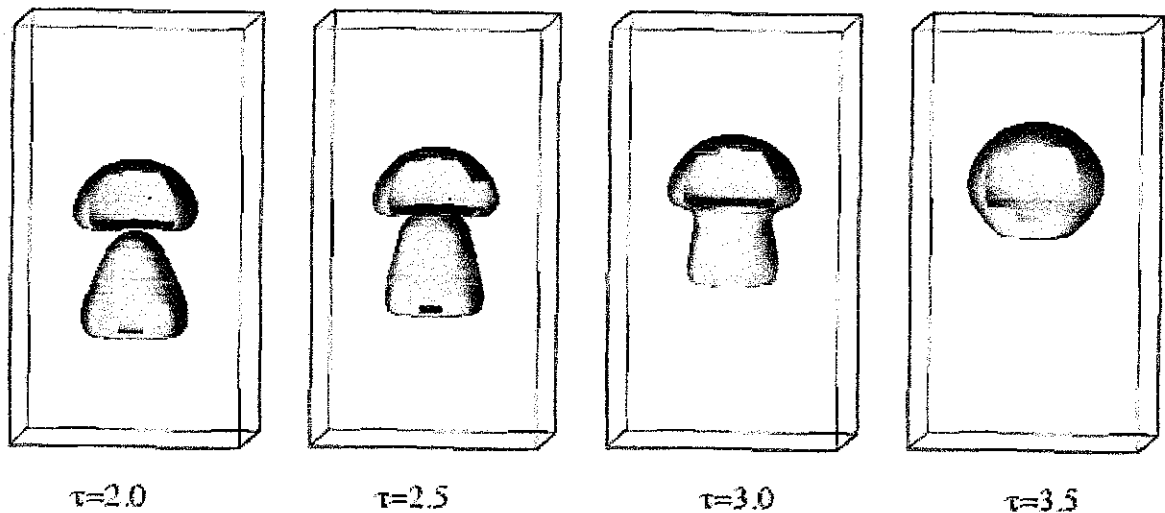
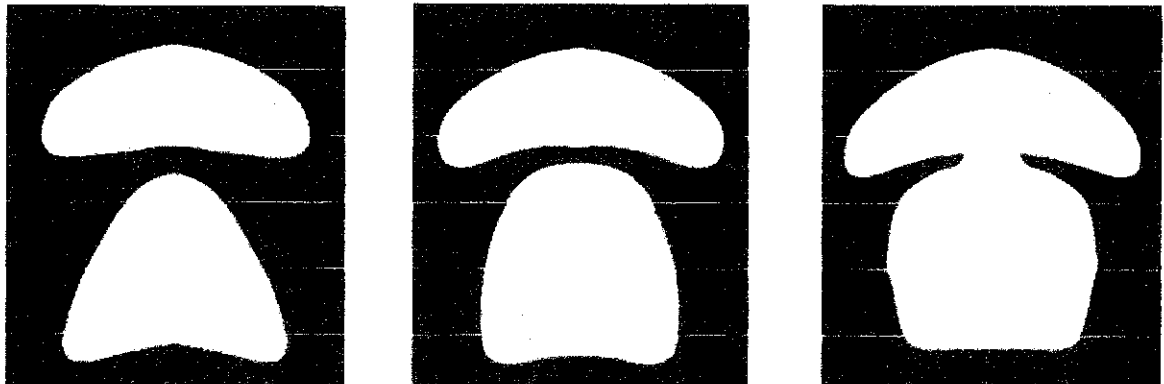
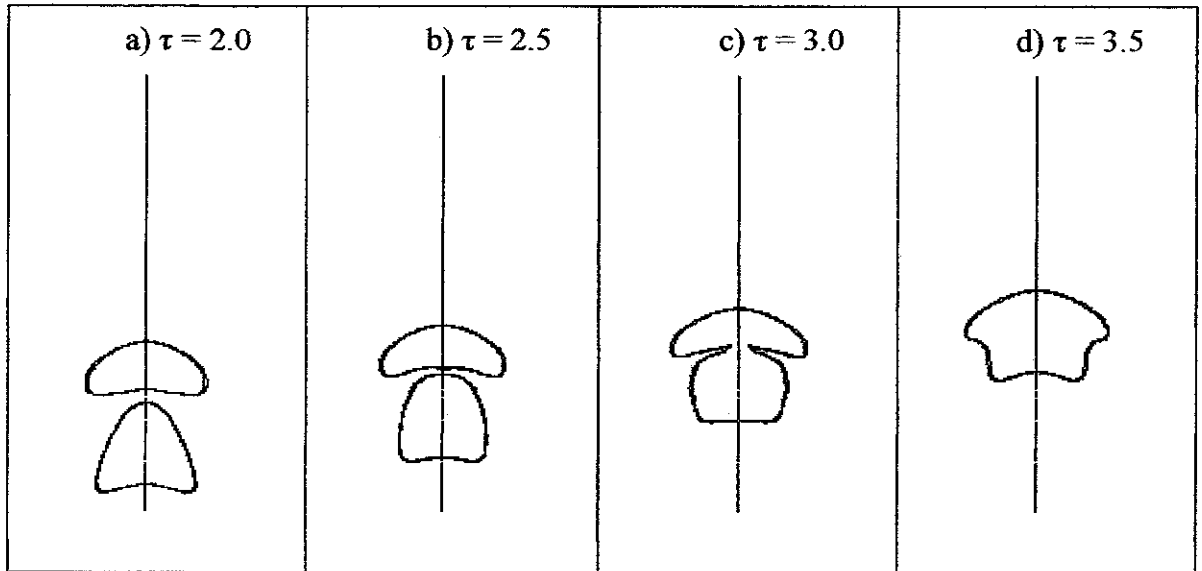


Figure 4.2.2: Predicted axisymmetric coalescence (Case 1)

(Re=10, Bo=5, $\rho_f/\rho_g=850$, $\mu_f/\mu_g=100$)

(Li Chen et al., 1998)



a) $\tau = 2.0$
($t = 0.010684$ s)

b) $\tau = 2.5$
($t = 0.013355$ s)

c) $\tau = 3.0$
($t = 0.016026$ s)

Figure 4.2.3: Simulated axisymmetric coalescence (Case 1)
($Re=10$, $Bo=5$, $\rho_f/\rho_g=850$, $\mu_f/\mu_g=100$)

Both Figure 4.2.2 and 4.23 show a part of contours of volume fraction series for development of bubble coalescence at $Re=10$ and $Bo=5$. The changes in the bubbles shape are carefully observed. The result obtained from CFD simulation (Figure 4.2.3) is compared with the predicted result from Li Chen et.al, 1998 (Figure 4.2.2). The outcome shows both results are closely agree with each other.

Based on the simulation result (Figure 4.2.3), the bubbles starts closely approaching each other at $\tau=2$. At this point, a pear-like shape is observed for the bottom (following) bubble. This happens due to the liquid jet behind the leading bubble which induces a severe deformation of the following bubble. The impact of the following bubble has terminates the vortex around the leading bubble, resulting a big circulation around those bubbles as a whole is gradually formed. Therefore, the liquid jet behind the leading bubble may be slightly smeared resulting in a spherical-cap-shaped leading bubble (Figure 4.2.3 a).

Meanwhile upon the collision, significant touch between those two bubbles then gives a mushroom-like shape in observation (Figure 4.2.3 c). When the two bubbles are in contact, because the surface tension always acts as a force reducing surface energy, the lower surface of the coalesced bubble is accelerated and a larger spherical cap is obtained (Figure 4.2.3 d).

The mechanism on bubble coalescence has been briefly explained in previous Section 4.1.2. Note that there is a distinct difference in shape changes between the results obtained in Figure 4.1.2 and the new result obtained in this section. As referring back to Figure 4.12, the two spherical bubbles became slightly ellipsoids in shape due to pressure difference between the top and bottom surfaces of the bubbles as the time progresses. However in the new result as shown in Figure 4.2.3, both bubbles change significantly in shape when coalesce. It is observed that this phenomenon happens because of the significant difference in the selection values of density ratio between those two simulations. The simulation result from Figure 4.12 is having $\rho_f / \rho_g = 1.25$, while we are having $\rho_f / \rho_g = 850$ for simulation indicated in Figure 4.2.3. Thus, it can be concluded that the density difference between gas and liquid may affect the behaviour of bubble coalescence in terms of mechanism (shape changes). Higher density ratio shows vigorous changes in shapes that may be caused by higher resultant liquid jet (pressure) between top and bottom of the bubbles.

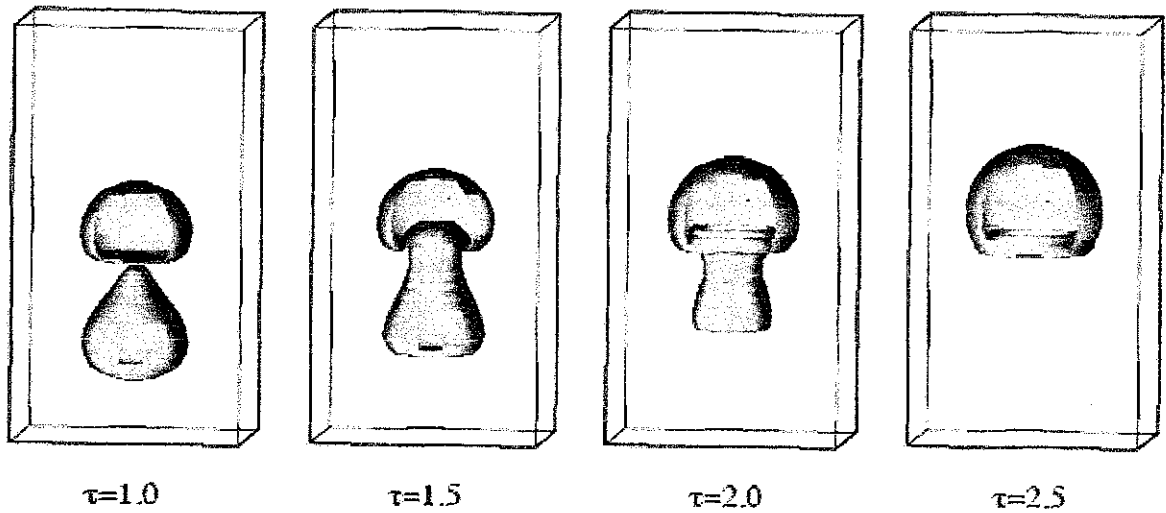


Figure 4.2.4: Predicted axisymmetric coalescence (Case 2)
 ($Re=10$, $Bo=50$, $\rho_f/\rho_g=850$, $\mu_f/\mu_g=100$)
 (Li Chen et al., 1998)

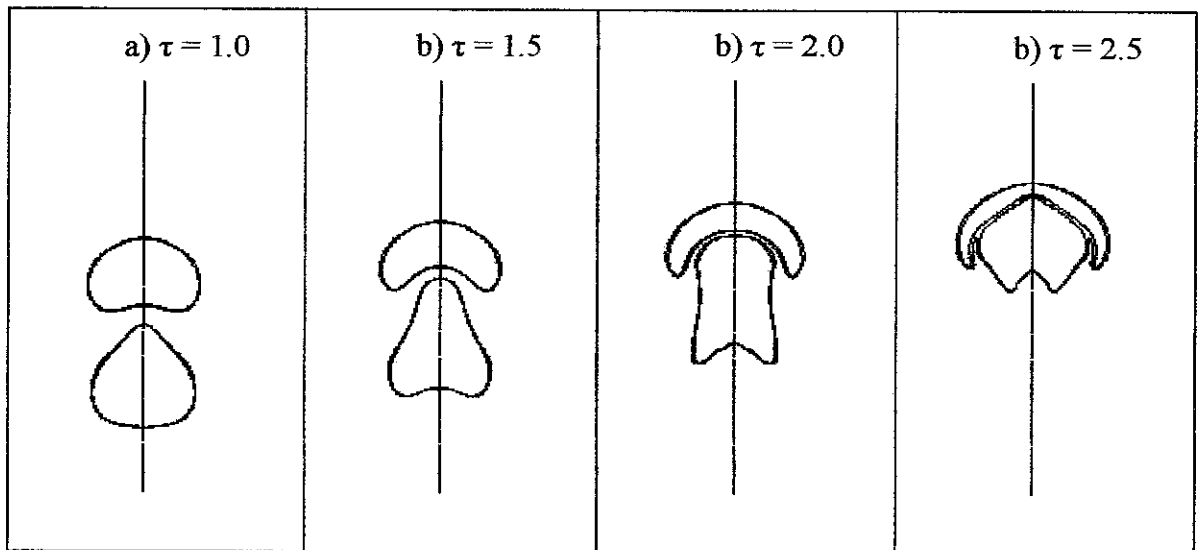


Figure 4.2.5: Simulated axisymmetric coalescence (Case 2)
 ($Re=10$, $Bo=50$, $\rho_f/\rho_g=850$, $\mu_f/\mu_g=100$)

For further validation, the simulation for $Re=10$ and $Bo=50$ also has been performed. The shapes changes and coalescence time can be observed. The result obtained from CFD simulation (Figure 4.2.5) is compared with the predicted result from

Li Chen et.al, 1998 (Figure 4.2.4). The outcome shows both results are closely agree with each other.

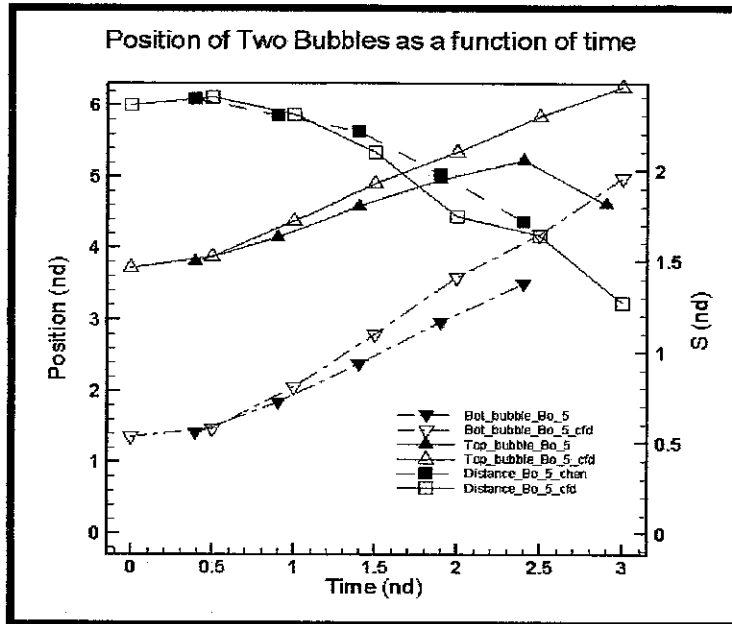


Figure 4.2.6: Position of two bubbles as a function of time (Case 1)
 ($Re=10$, $Bo=5$, $\rho_f/\rho_g=850$, $\mu_f/\mu_g=100$)

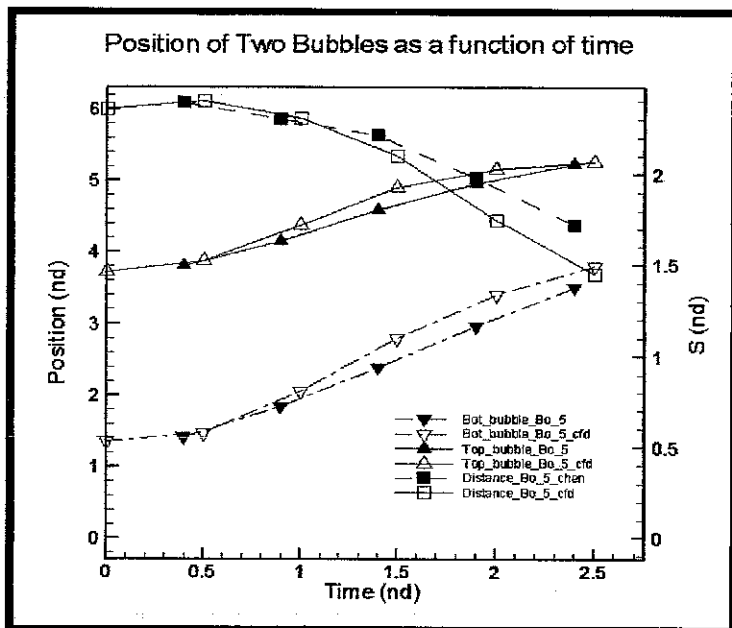


Figure 4.2.7: Position of two bubbles as a function of time (Case 2)
 ($Re=10$, $Bo=50$, $\rho_f/\rho_g=850$, $\mu_f/\mu_g=100$)

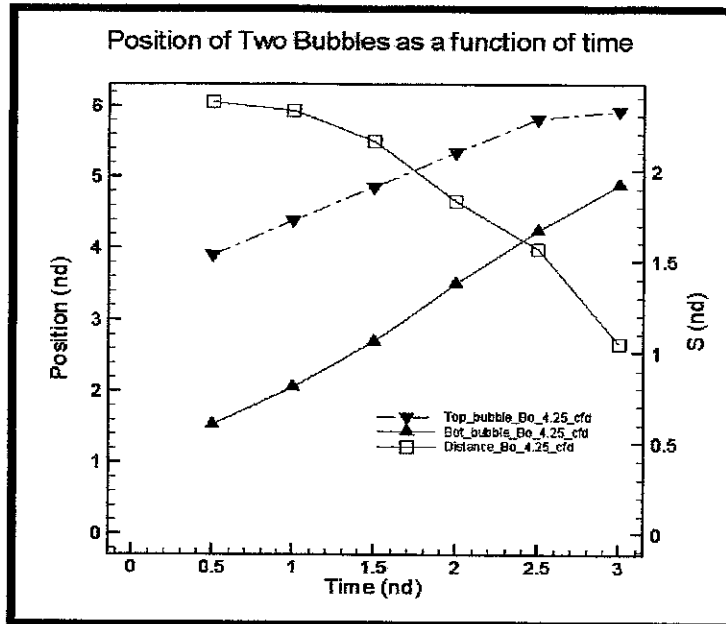


Figure 4.2.8: Position of two bubbles as a function of time (Case 3)
 $(Re=8.5, Bo=4.25, \rho_f / \rho_g=850, \mu_f / \mu_g=100)$

Figure 4.2.6, 4.2.7 and 4.2.8 show the position of two bubbles as a function of time for the defined cases. Figure 4.2.6 and 4.2.7 show the simulation at $Re=10$ with different Bond number; $Bo=5$ and $Bo=50$ respectively. These results validate the mother paper given by Li Chen et al., 1998 and show a closed agreement between each other. From the both graphs, it is observed that both bubbles start to rise and approach each other as the time progresses. Otherwise, it is also observed that the distance between the two bubbles is getting smaller until the bubbles coalesced.

The bubbles coalesced estimated at $\tau=3.0$ for $Bo=5$ and $\tau=2.5$ for $Bo=50$. The bubbles with a high Bond number, $Bo=50$ (which indicates low surface tension) merge earlier than the bubbles with low Bond number, $Bo=5$ (which indicates high surface tension). At a low surface tension, the two bubbles deformed more while approaching due to stronger liquid jet behind both bubbles. This also results a rapid rise of the two bubbles at the beginning. Otherwise, a high surface tension produces a weak liquid jet behind the bubbles. Furthermore, the surface tension force is always trying to maintain a shape having a minimum surface energy, which makes the stretching of the top surface of the following bubble harder (Li Chen et al., 1998). These all cause a late coalescence to occur.

CHAPTER 5

CONCLUSION AND RECOMMENDATION

5.1 Conclusion

The dynamics of bubble coalescence process of two co-axial bubbles within liquid phase under laminar flow condition has been studied by using Computational Fluid Dynamic. The modelling approach selected in this project is Volume-of-Fluid method (VOF) which commonly used to analyse the dynamic and deformation of the liquid-gas interface.

It is obtained that mechanism of bubble coalescence is in reasonable agreement with the existing theory available in the established literature. From the result, the consecutive steps in bubble coalescence can be described into three distinct steps; (1) collision of bubbles, (2) trapping and thinning of a thin liquid film and (3) film rupture (Oolman, T. O. and Blanch, H. W., 1986; Rahman Sudiyo). The result also shows that the density difference between gas and liquid may affect the behaviour of bubble coalescence in terms of mechanism (shape changes). Higher density ratio shows vigorous changes in shapes that may be caused by higher resultant liquid jet (pressure) between top and bottom of the bubbles.

Futhermore, the effect of surface tension on the coalescence have been studied as one of the objectives. From the result, a high surface tension is observed to produce a weak liquid jet behind the bubbles. In addition, the resultant high surface tension force prohibits the surface stretching. These all cause a late coalescence to occur.

Moreover, from the result generated by CFD, the bubble trajectories can be plotted accurately and such an information should help in hydrodynamics modelling of bubbly flows. In conclusion, all the project objectives are sastified.

5.2 Recommendation and Future Works

Recommendation and future work to improve the efficiency and to gain better insight of the project are stated as following;

- Perform numerous simulations to study various affecting factors on bubble coalescence which includes liquid viscosity, bubble size and bubble spacing.
- Investigate the dynamics of bubble coalescence with different initial bubble position, namely side by side rising bubbles. For this purpose, a validation case has already been considered and simultaneously been run. However, the ultimate result still cannot be obtained due to high computational power demand.

REFERENCES

- [1] E. I. V. van den Hengel, N. G. Deen, and J. A. M. Kuipers, 2005, "Application of Coalescence and Breakup Models in a Discrete Bubble Model for Bubble Columns" *Ind. Eng. Chem. Res.*, **44**: 5233-5245
- [2] Katerina A. Mouza, Nikolaos A. Kazakis and Spiros V. Paras, 2004, "Bubble Column Reactor Design Using A CFD Code" *1st International Conference: From Scientific Computing to Computational Engineering*
- [3] Sanada Toshiyuki, Sato Ayaka, Shirota Minori and Watanabe Masao, 2009, "Motion and coalescence of a pair of bubbles rising side by side," *Chemical Engineering Science* **64** (11): 2659-2671
- [4] Li Chen, Yuguo Li and Richard Manasseh, 1998, "The coalescence of bubbles – a numerical study," *Third International Conference on Multiphase Flow, ICMF'98 Paper 626*
- [5] S. Hardt, 2005, "An extended volume-of-fluid method for micro flows with short-range interactions between fluid interfaces" *Physics of Fluids*, **17**, 100601
- [6] Todd Thorsen, Richard W. Roberts, Frances H. Arnold, and Stephen R. Quake, 2001, "Dynamic Pattern Formation in a Vesicle-Generating Microfluidic Device" *Physical Review Letters*, **86**, Num.18
- [7] *Unknown author*. Retrieved on 12 Sept 2009
<<http://www.lmnoeng.com/fluids.htm>>.
- [8] *Unknown author*. Retrieved on 12 Sept 2009
<<http://www.usetute.com.au/molpolar.html>>.
- [9] Michael Spyridopoulos, Stefaan Simons, Stephen Neethling and Jan Cilliers, 2004, "Effect of humic substances and particles on bubble coalescence and foam stability in relation to dissolved air flotation processes," *Physicochemical Problems of Mineral Processing* **38**: 37-52
- [10] Kathryn Tse, Thomas Martin, Caroline M. Mcfarlane and Alvin W. Nienow, 1998, "Visualisation of bubble coalescence in a coalescence cell, a stirred tank and a bubble column," *Chemical Engineering Science* **53** (23): 4031-4036

- [11] Lessard R.R. and Ziemiski S.A, 1971, "Bubble coalescence and gas transfer in aqueous electrolytic solutions," *Ind. Engineering Chem. Fund* **10**: 260-269
- [12] Chesters A.K., 1991, "The modelling of coalescence processes in fluid-liquid dispersions: a review of current understanding," *Trans. I. Chem. E.* **69, Part A**: 259-270
- [13] Marrucci G. and Nicodemo L., 1967, "Coalescence of gas bubbles in aqueous solutions of inorganic electrolytes," *Chemical Engineering Science* **22**: 1257-1265
- [14] N.A Kazakis, A.A. Mouza, and S.V. Paras, 2008, "Coalescence during bubble formation at two neighbouring pores: An experimental study in microscopic scale," *Chemical Engineering Science* **63**: 5160-5178
- [15] W. Kracht and J.A. Finch, 2009, "Using sound to study bubble coalescence," *Journal of Colloid and Interface Science* **332**: 237-245
- [16] André Bakker, 2002, "Applied Computational Fluid Dynamics"
- [17] Dmitri Kuzmin, n.d., "Introduction to Computational Fluid Dynamics"
- [18] *Fluent Manual*, 2003, Fluent Inc.
- [19] J.M. Martinez, X. Chesneau and B. Zeghmami, n.d., "Numerical and experimental studies of air bubbles coalescence in a quiescent water column"
- [20] Oolman, T. O. and Blanch, H. W., 1986, "Bubble coalescence in stagnant liquids", *Chem. Engng Commun* **43**: 237-261
- [21] Pilon, Laurent, Viskanta, and Raymond, 2004, " Superficial gas velocity for onset of foaming" *Chemical Engineering and Processing*, **43 (2)**: 149-160.
- [22] Rahman Sudiyo, n.d., "Bubble Coalescence and Breakup in Gas-Liquid Stirred Tank Reactors"
- [23] Duineveld, P.C., 1998, "Bouncing and coalescence of bubble pairs rising at high Reynolds number in pure water or aqueous surfactant solutions" *Appl. Sc. Res*, **58**: 409-439
- [24] Chesters, A.K and Hofman, G., 1982, "Bubble coalescence in pure liquids" *Appl. Sc. Res*, **38**: 353-361

- [25] Deen, N. G., M. v. S. Annaland, et al, 2009, "Direct numerical simulation of complex multi-fluid flows using a combined front tracking and immersed boundary method" *Chemical Engineering Science*, **64** (Compendex): 2186-2201
- [26] Iaccarino, G. and R. Verzicco, 2003, "Immersed boundary technique for turbulent flow simulations" *Applied Mechanics Review*, **56** (Compendex): 331-347
- [27] Fadlun, E. A., R. Verzicco, et al, 2000, "Combined Immersed-Boundary Finite-Difference Methods for Three-Dimensional Complex Flow Simulations" *Journal of Computational Physics*, **161**(1): 35-60
- [28] J Mohd-Yusof, 1998, "Development of immersed boundary methods for complex geometries" *Center for Turbulence Research: Annual Research Briefs*
- [29] Claudio P. Ribeiro Jr., Dieter Mewes, 2006, "On the effect of liquid temperature upon bubble coalescence" *Chemical Engineering Science*, **61** (17): 5704-5716
- [30] I. B. Bazhlekov, A. K. Chesters, F. N. van de Vosse, 2000, "The effect of the dispersed to continuous-phase viscosity ratio on film drainage between interacting drops" *International Journal of Multiphase Flow*, **26** (3): 445-466
- [31] Ryszard Pohorecki, Wladyslaw Moniuk, Pawel Bielski, Artur Zdrojkowski, 2001, "Modelling of the coalescence/redispersion processes in bubble columns" *Chemical Engineering Science*, **56** (21-22): 6157-6164
- [32] Manasseh, R., Yoshida, S. and Rudman, M., 1998, "Bubble formation processes and bubble acoustic signals", *ICMF'98, France, June 8-12*.
- [33] The Engineering Toolbox. Retrieved on 12 April 2010
<http://www.engineeringtoolbox.com/specific-heat-ratio-d_602.html>.

APPENDICES

APPENDIX A

Specific Heat Ratio of Air (at Standard Atmospheric Pressure in SI Units)

Temperature - t - °C	Specific Heat Ratio $\gamma = c_p/c_v$
-40	1.401
-20	1.401
0	1.401
5	1.401
10	1.401
15	1.401
20	1.401
25	1.401
30	1.400
40	1.400
50	1.400
60	1.399
70	1.399
80	1.399
90	1.399
100	1.397
200	1.390
300	1.379
400	1.368
500	1.357
1000	1.321

(http://www.engineeringtoolbox.com/specific-heat-ratio-d_602.html)